^{11}C-Methionine PET of Myocardial Inflammation in a Rat Model of Experimental Autoimmune Myocarditis

Yoshifumi Maya*[1,2], Rudolf A. Werner*[1,3,4], Claudia Schütz[3,5], Hiroshi Wakabayashi[1], Samuel Samnick[1,3], Constantin Lapa[1], Christina Zechmeister[3,5], Roland Jahns[3,6], Valérie Jahns†[3,5], and Takahiro Higuchi†[1,3]

[1]Department of Nuclear Medicine, University of Würzburg, Würzburg, Germany; [2]Research Centre, Nihon Medi-Physics Co., Ltd., Chiba, Japan; [3]Comprehensive Heart Failure Center, University of Würzburg, Würzburg, Germany; [4]Else–Kröner–Forschungskolleg, Interdisciplinary Center for Clinical Research, University of Würzburg,Würzburg, Germany; [5]Department of Pharmacology, University of Würzburg, Würzburg, Germany; and [6]Interdisciplinary Bank of Biomaterials and Data Würzburg (IBDW), University of Würzburg, Würzburg, Germany

For correspondence contact: Takahiro Higuchi, Department of Nuclear Medicine/Comprehensive Heart Failure Center, University of Würzburg, Oberdürrbacher Strasse 6, 97080 Würzburg, Germany.
E-mail: thiguchi@me.com
*Contributed equally to this work.
†Contributed equally to this work.

Myocarditis is an inflammatory disease of the heart muscle that is pathologically characterized by the infiltration of the myocardium by immune cells such as T cells and macrophages. Still, it is a major cause of dilated cardiomyopathy and sudden cardiac death in younger adults (*1–4*). The clinical presentation of myocarditis is highly variable and associated with a wide range of symptoms, such as dyspnea, chest pain, and cardiac arrhythmia (*3,5*). Therefore, diagnosis solely based on the clinical presentation is challenging. Endomyocardial biopsy is considered the gold standard for definite diagnosis of myocarditis; however, this highly invasive approach is associated with inherent sampling error, limiting its sensitivity (*6*). Therefore, in patients with suspected myocarditis noninvasive imaging may play a pivotal role for rapid initial diagnosis, biopsy guidance to increase diagnostic sensitivity, and therapy monitoring and adaptation/optimization of therapeutic strategies. Among the available imaging modalities, cardiac MRI has been proven to be a useful tool for the assessment of myocardial inflammation (*7*) because it allows for high-resolution measurements of ventricular morphology, function, and tissue characterization of the myocardium (*8–10*). In addition, irreversible myocardial injury, such as necrosis and fibrosis, can be visualized by late gadolinium enhancement (*8,11,12*). However, standard MRI may be insensitive for the detection of inflammatory activity, which is critical for monitoring therapeutic responses to prevent secondary tissue alterations. On the other hand, PET is a highly sensitive, noninvasive technology that can be applied to visualize target-specific molecules using appropriate positron-emitting radioactive tracers (*13*). This technology is promising for the quantitative detection of myocardial alterations such as immune cell infiltration, even at early stages of myocarditis before structural alternations can be visualized by other morphologic imaging modalities.

L-[methyl-^{11}C]methionine (^{11}C-methionine) has been widely used for diagnosis of various cancers, such as brain tumors (*14*) and multiple

myeloma (*15*). Recently, several experimental studies have suggested the potential of ^{11}C-methionine PET to detect inflammatory lesions (*16,17*). Kubota et al. reported that methionine uptake is increased in macrophages that invade tumor lesions (*18*). By conducting in vitro binding experiments using isolated inflammatory cells, Oka et al. further confirmed that L-[methyl-^{14}C]methionine (^{14}C-methionine) accumulates in inflammatory cells, including macrophages, T cells, and B cells (*19*).

In the present study, we aimed to explore the usefulness of radiolabeled methionine for the assessment of cardiac inflammatory lesions in a rat model of autoimmune myocarditis.

MATERIALS AND METHODS

All reagents were commercial products and used without further purification unless otherwise indicated. Animal studies were approved by the local institutional animal care and use committee and performed according to the *Guide for the Care and Use of Laboratory Animals* published by the U.S. National Institutes of Health (NIH publication 85-23, revised 1996 (*20*)).

Radiochemistry

^{14}C-methionine was purchased from PerkinElmer. ^{11}C-methionine and ^{18}F-FDG were produced in-house with a 16-MeV Cyclotron (PETtrace 6; GE Healthcare), as described previously (*21*). Briefly, ^{18}F-FDG was produced on a FASTlab synthesizer (GE Healthcare), and ^{11}C-methionine was synthesized on a TRACERlab FX-C Pro module (GE Healthcare) by an online ^{11}C-methylation of L-homocysteine. ^{18}F-fluorobenzyl triphenyl phosphonium, a myocardial perfusion PET tracer, was prepared as reported previously (*22,23*). All radiolabeled ligands were analyzed by high-performance liquid chromatography or thin-layer chromatography at the end of syntheses to confirm radiochemical identity and purity (>95%).

Animal Model of Myocarditis

EAM was induced in female Lewis rats (Charles River Laboratories; weighing 200–250 g) as previously described (*24,25*), with some minor modifications. Briefly, 0.5 mg/mL of pig cardiac myosin (0.25 mL; Sigma Aldrich) in an equal volume of complete Freund adjuvant (Difco) supplemented with *Mycobacterium tuberculosis* (Difco) was injected subcutaneously into the backs (3 different sites) of 15 rats on days 0 and 7. Control rats (n = 9) were injected with adjuvant alone. Imaging experiments were performed on day 21 after the first immunization.

Ex Vivo Dual-Tracer Autoradiography

Dual-tracer autoradiography was conducted with ^{14}C-methionine and ^{18}F-FDG (*26*). ^{18}F-FDG (37 MBq) was injected intraperitoneally into conscious rats (n = 4) after a 14-h fasting period to minimize physiologic cardiac glucose uptake. Subsequently, ^{14}C-methionine (0.74 MBq) was injected via the tail vein 40 min after the ^{18}F-FDG injection. Tracer distribution times before euthanasia were 60 min for ^{18}F-FDG and 20 min for ^{14}C-methionine. The heart was extracted, frozen, and cut into 20-μm short-axis slices using a cryostat (Leica). First, the imaging plate (Multi Sensitive Phosphor Screens; PerkinElmer) was exposed for 60 min to visualize the distribution of ^{18}F-FDG with a digital autoradiography system (CR 35 Bio; Raytest). After 48 h to allow for the decay of ^{18}F, the same preparations were exposed again for 30 d to measure ^{14}C-methionine uptake. After autoradiography, the same tissue slices were stained with standard hematoxylin and eosin staining. Quantitative analysis of the digital autoradiographic images was performed with image analysis software (Raytest). Regions of interest (ROIs) were placed on the mid-ventricular short-axis cardiac images to cover the whole area of the section and were visually classified into 3 types based on the corresponding histologic findings of hematoxylin and eosin staining: control areas (nonimmunized rat hearts, n = 21), noninflammatory areas (<3% myocardial inflammatory lesions in immunized rat hearts, n = 20), and inflammatory areas (>3% myocardial inflammatory lesions, n = 41). The respective activities of ^{14}C and ^{18}F were calculated using identical ROI sets. Obtained activity values were normalized for the injected dose and expressed as the background-corrected quantum levels per unit area (QL/pixel).

Immunohistochemistry

Immunohistologic analysis of cardiac tissues was performed using 7-μm slices adjacent to the short-axis slices used for autoradiographic analysis. Immunohistochemical staining was performed using standard techniques. Briefly, tissue sections were fixed (10-min acetone) and blocked with 10% bovine serum albumin. The sections were then incubated overnight with either rabbit anti-CD68 (Abcam) or rabbit anti-CD3 (Abcam) antibodies. Biotinylated goat antirabbit IgG (Thermo Fisher Scientific) was used as a secondary antibody. Optical microscopy images were obtained using a Keyence BZ-9000 microscope (Keyence Corp.). To quantify the percentage of an area having CD68-positive myocardial areas, ROIs were set on the anterior, lateral, inferior, and septal left ventricular wall as well as right ventricular wall (Fig. 1D). The percentage of CD68-positive areas within each ROI was determined by

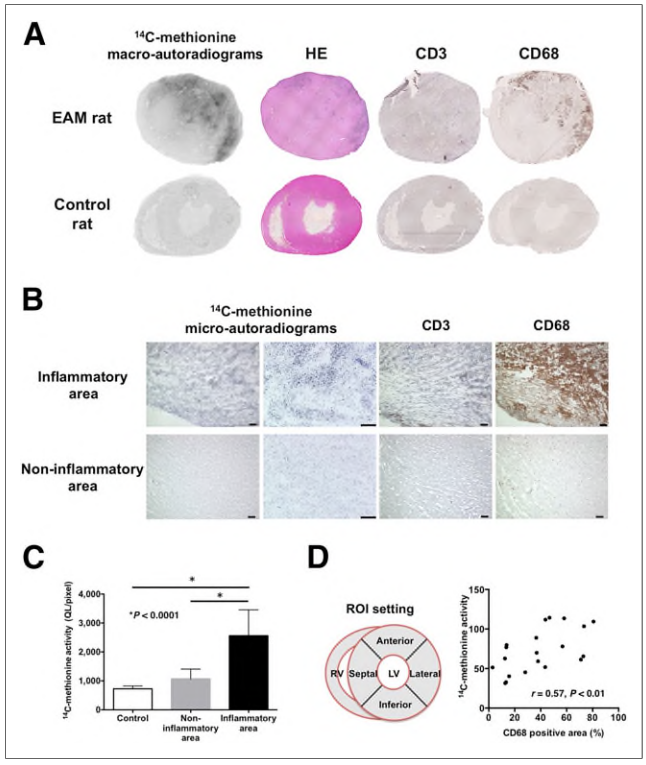

FIGURE 1. (A) Exemplary images of mid-ventricular short-axis slices of an EAM rat heart and a control rat. Intense focal myocardial ^{14}C-methionine uptake was noted in macroautoradiograms of EAM rats. ^{14}C-methionine uptake matched well with CD68-positive macrophage infiltrates. (B) Microautoradiograms with hematoxylin counterstaining and CD3 and CD68 immunohistochemistry to analyze subcellular tracer distribution. Precise localization of tracer signals and cellular infiltrates are shown. Scale bar = 100 μm. (C) ^{14}C-methionine activity was significantly higher in inflamed (black bar) than noninflamed myocardial areas (gray bar) or hearts from control animals (white bar). QL/pixel = background-corrected quantum levels per unit area. (D) High ^{14}C-methionine uptake correlated strongly with CD68 signals of positively stained myocardial areas (in %). HE = hematoxylin and eosin staining; RV = right ventricle; LV = left ventricle.

computer-aided image analysis (Image J software, version 1.47v; National Institutes of Health) using an intensity threshold that matched the visually identified CD68-positive staining area as closely as possible. Then, the correlation between the histologically CD68-positive areas and the intensity of ^{14}C-methionine uptake was analyzed.

Microautoradiography

High-resolution microautoradiography was used to assess the distribution of ^{14}C-methionine at the microscopic level. ^{14}C-methionine–radiolabeled sections were dipped into the liquid emulsion (NTB-2; Kodak) at 43°C. The slides were air-dried for 5 h at room temperature and exposed in the dark at 4°C for 1 mo. The sections were then developed (D-19 developer [Kodak], 5 min), washed in pure water, fixed (Kodak Fixer, 10 min), and washed again (pure water, 2 × 5 min). The tissue sections were counterstained with hematoxylin for 2 min, and optical microscopy images were taken using a microscope (BZ-9000; Keyence).

In Vivo PET Imaging

A dedicated small-animal PET scanner (Inveon; Siemens) was used to explore the feasibility of in vivo detection of myocardial inflammation by ^{11}C-methionine imaging. All animals were maintained under anesthesia with 2% isoflurane during PET image acquisition. ^{11}C-methionine (50 MBq) was injected intravenously into EAM rats ($n = 6$) and control animals ($n = 5$), and 30 min after tracer injection data acquisition was initiated for a period of 7 min. Dynamic PET imaging over 40 min, beginning at the time of tracer administration, was performed with exemplary EAM rats. Because a tracer with a short physiologic half-life (^{11}C, 20 min) was used, only 2 dynamic PET scans were obtained. After completion of ^{11}C-methionine PET, ^{18}F-FDG PET was conducted with an interval of more than 4 half-lives of ^{11}C decay. Sixty minutes after intraperitoneal administration of ^{18}F-FDG (37 MBq), PET images were acquired over a period of 7 min. Subsequently, ^{18}F-fluorobenzyl triphenyl phosphonium myocardial PET was performed as a reference for the heart location (*23*).

Data Analysis of PET

PET images were analyzed by AMIDE-bin, version 1.0.2 (*27*). ROIs were drawn manually on the left ventricular wall in a mid-ventricular short-axis slice. The mean concentration of radioactivity within the ROIs was expressed as the percentage injected dose per tissue cubic centimeter (%ID/cm^3). To analyze the correlation between ^{11}C-methionine and ^{18}F-FDG uptake, both images were carefully coregistered, and ROIs were set on the anterior, lateral, inferior, and septal left ventricular wall and right ventricular wall to cover the whole slice. Within identical ROIs, the respective uptake values (%ID/cm^3) of each tracer were calculated. In the dynamic PET study, list-mode data were reconstructed into a dynamic sequence (25 frames: 15 × 8, 3 × 60, and 7 × 300 s) using ordered-subset expectation maximization with 16 subsets and 4 iterations. Decay-corrected time–activity curves were generated for myocardial tissue and blood input function, respectively. A partial-volume effect correction was not performed in the present study because a widely accepted method for the heart of a small animal has not yet been established.

Statistical Analysis

Statistical analysis was performed using PRISM software (GraphPad Software). Results are given as mean ± SD. Normality of the data and equality of variances were checked by the Kolmogorov–Smirnov and Brown–Forsythe tests, respectively. Multiple comparisons were performed by the Kruskal–Wallis test and Dunn multiple-comparison test to evaluate differences in ^{14}C-methionine uptake in healthy myocardium (control rats), noninflammatory myocardial areas, and acute inflammatory lesions. Comparisons of uptake ratios of ^{14}C-methionine and ^{18}F-FDG between acute inflammatory lesions and the noninflammatory areas were compared by the paired Student *t* tests. Unpaired Student *t* tests were used to assess the differences in ^{11}C-methionine uptake between EAM rats and control animals. Correlations were calculated using Spearman rank correlation. A P value of less than 0.05 was considered statistically significant.

RESULTS

Determination of ^{14}C-Methionine Uptake by Macro- and Microautoradiography

Postmortem analysis macroscopically showed enlarged hearts with discolored surfaces in 10 of 15 (67%) EAM rats. Subsequently, multiple focal cardiac inflammatory lesions were histologically identified by hematoxylin and eosin staining in EAM rats, whereas no lesions were detected in control animals (Fig. 1A). In addition, macroautoradiographic images clearly demonstrated high-density focal cardiac ^{14}C-methionine accumulation in EAM rats, but no relevant regional tracer uptake in control rats (Fig. 1A). ^{14}C-methionine uptake was almost confined to inflammatory cells in light microscopy images (Fig. 1B). Quantitative analysis of macroautoradiography showed that ^{14}C-methionine uptake was significantly higher in the histologically identified inflammatory lesions (2,561 ± 894 QL/pixel) than in the remote noninflammatory areas (1,068 ± 339 QL/pixel; $P < 0.0001$) or control hearts (727 ± 97 QL/pixel; $P < 0.0001$; Fig. 1C).

Correlation with Immunohistologic Analysis

Correlations of ^{14}C-methionine uptake with immunohistologic findings were analyzed in serial cardiac sections stained with anti-CD3 and anti-CD68 antibodies. On the basis of the results of our immunostainings, approximately 70% of the cells present in the inflammatory lesions were macrophages (Figs. 1A and 1B), whereas only a small number of CD3-positive T cells was observed. An increase in ^{14}C-methionine uptake was noted in the CD68-positive myocardial areas (Figs. 1A and 1B). Furthermore, quantitative analysis yielded a rather good correlation between ^{14}C-methionine signal intensity and CD68 positivity (percentage positively stained areas; $r = 0.57$; $P < 0.01$; Fig. 1D).

Comparison of ^{14}C-Methionine and ^{18}F-FDG Distribution

Analysis of dual-tracer autoradiograms showed a congruent distribution pattern of ^{14}C-methionine and ^{18}F-FDG (Fig. 2A). Quantitative analysis yielded a strong positive correlation between the signal intensity of ^{14}C-methionine and ^{18}F-FDG uptake ($r = 0.96$; $P < 0.0001$; Fig. 2B). The contrast between inflammatory and noninflammatory myocardial areas was slightly higher for ^{18}F-FDG than for ^{14}C-methionine (3.45 ± 0.68 vs. 2.07 ± 0.21, respectively; $P < 0.05$; Fig. 2C).

In Vivo PET Imaging

^{11}C-methionine PET revealed a high focal uptake in the hearts of EAM rats, whereas no cardiac tracer uptake was observed in the hearts of control animals (Fig. 3A). The average tracer uptake (%ID/cm^3) was significantly higher in EAM hearts than in control hearts (0.64 ± 0.09 vs. 0.28 ± 0.02, respectively; $P < 0.001$; Fig. 3B). Tracer uptake in the thymus and the liver was similar in both EAM and control rats, indicating physiologic tracer distribution.

The time course of cardiac ^{11}C-methionine distribution determined by in vivo PET analysis of an EAM rat over a period of 40 min is shown in Figure 3C. The time–activity curve revealed a constantly increasing focal tracer accumulation in the heart of EAM rats together with a rapid clearance from the blood. Focal cardiac ^{11}C-methionine uptake reached a plateau approximately 10 min after tracer injection and, thereafter, remained constant.

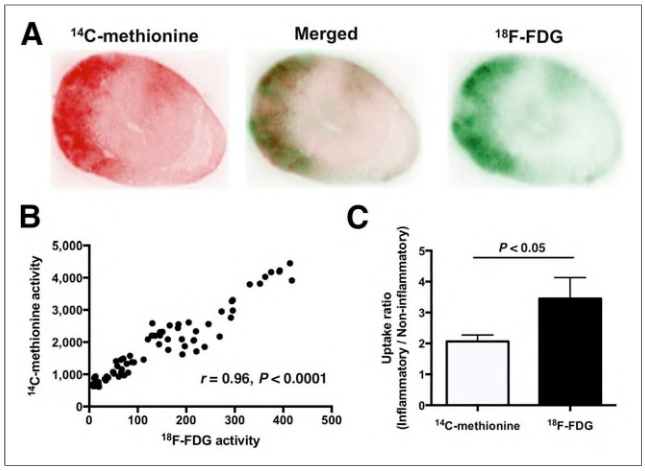

FIGURE 2. Direct comparison of ^{14}C-methionine and ^{18}F-FDG distribution by dual-tracer autoradiography. (A) Representative mid-ventricular short-axis images of EAM rat. Myocardial areas with ^{14}C-methionine and ^{18}F-FDG uptake are well matched. (B) Excellent correlation between ^{14}C-methionine and ^{18}F-FDG uptake was determined. (C) Uptake ratio of inflamed versus noninflamed myocardial areas was significantly higher for ^{18}F-FDG (black bar) than for ^{14}C-methionine (white bar).

PET images demonstrating colocalization of ^{11}C-methionine and ^{18}F-FDG in the same rats are shown in Figure 4A. Quantitative analysis of PET images revealed a strong positive correlation between ^{11}C-methionine and ^{18}F-FDG uptake ($r = 0.82$; $P < 0.0001$; Fig. 4B).

DISCUSSION

The results of our study demonstrate the potential feasibility of an assessment of cardiac inflammation by radiolabeled methionine. In EAM rats, ex vivo tissue analysis revealed increased focal ^{14}C-methionine accumulation in histologically proven myocardial inflammatory lesions. Furthermore, focally increased tracer uptake matched well with focal macrophage infiltration as determined by CD68 immunohistochemical staining. In vivo PET studies allowed the focal ^{11}C-methionine signal in EAM hearts to be followed.

EAM rats fairly well mimic human myocarditis in the acute and chronic phases (*28*). To date, several groups have reported induction of autoimmune myocarditis by immunization in the rear footpad using a combination of porcine cardiac myosin and Freund complete adjuvant (*24,25*). These EAM rats developed myocardial inflammatory cell infiltrates beginning 12–14 d after the first immunization, with a peak around day 21 (*29*). Immunohistologically, macrophages and CD4-positive T cells are the predominant cell types present in the early infiltrates (*30,31*). To reduce the distress of antigen administration into the footpad, Schmerler et al. immunized rats subcutaneously into the neck and flanks. They reported minor morbidity (22%) and milder inflammation of the myocardium than in rats receiving footpad injections (*25*). In the present study, we modified the previously published protocol and succeeded in generating an EAM model that exhibited high morbidity (67%) at 21 d after immunization. Consistent with other EAM models, we found that macrophages accounted for the majority of infiltrating cells with a small number of CD3-positive T cells (*25,30,32*). All experiments in the present study were performed only at the peak of inflammation (day 21 after the first immunization); however, in a future study, data at different time points should also be obtained to evaluate the usefulness across a wide variety of severities and various types of inflammatory cells.

In addition to the myosin-induced EAM model, a virus-induced myocarditis model has also been reported (*29,33,34*), which has only been established in mice, however. Because of the limited resolution of small-animal PET imaging, rat models have the great advantage of better image quality.

In our ex vivo autoradiography studies, the uptake of ^{14}C-methionine in inflammatory lesions was significantly higher than that in remote noninflammatory areas and in control hearts. Furthermore, the strong positive correlation between ^{14}C-methionine uptake (autoradiography) and CD68-positive signals (immunohistochemistry) suggests that ^{14}C-methionine accumulates mainly in macrophages. We observed a slight increase in tracer uptake in noninflamed myocardial areas compared with the control hearts of nonimmunized animals, although this increase was not statistically significant. Because CD68 immunostaining revealed a small number of macrophages even in remote noninflamed myocardial areas of our EAM rats (Fig. 1B), in the present EAM model, we assume that minor nontargeted macrophage penetration also occurred in myocardial areas near the inflamed core areas.

In the present study, ^{14}C-methionine accumulation was assessed using microautoradiography. Microautoradiography is a classic technique that enables elucidation of the tracer distribution at the cellular level, providing high-resolution images using light microscopy (*35*). ^{14}C-methionine accumulation in inflammatory cell infiltrates could be well documented at the microscopic level. Furthermore, from CD68 immunohistochemical staining of the respective adjacent cardiac sections, it could be inferred that macrophages represented most of the infiltrating cells.

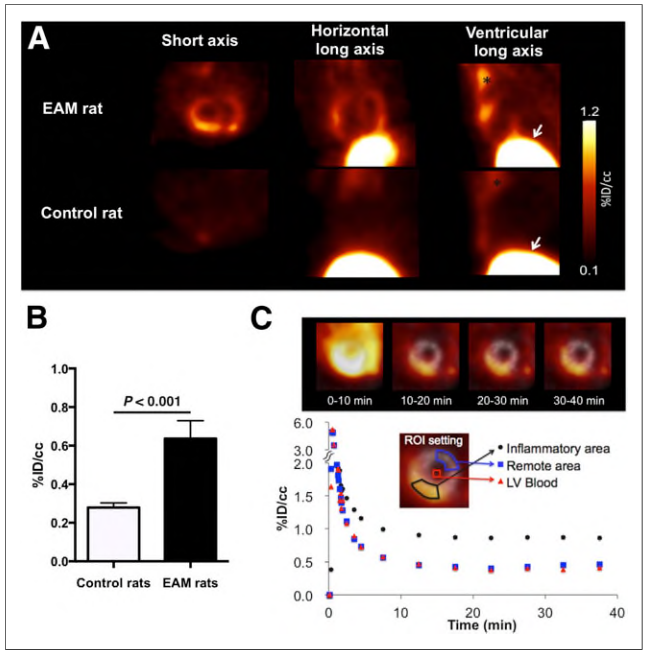

FIGURE 3. (A) Representative ^{11}C-methionine PET images 30 min after intravenous tracer administration. Strong focal cardiac ^{11}C-methionine uptake was observed in EAM rats but not in control animals. Extracardiac tracer accumulation in thymus (asterisk) and the liver (arrowheads) was noted in both EAM and control rats, whereas respective tracer activities in lungs and blood pool were rather low. (B) Cardiac tracer uptake in EAM rats (black bar) was significantly higher than that in control rats (white bar). (C) Representative short-axis PET images and time–activity curves of dynamic PET imaging in EAM rat. Ten to 20 min after administration, tracer uptake increased in heart together with rapid clearance of blood activity. Cardiac signals remained stable for 30–40 min. Gray scale images serve as reference for location of heart.

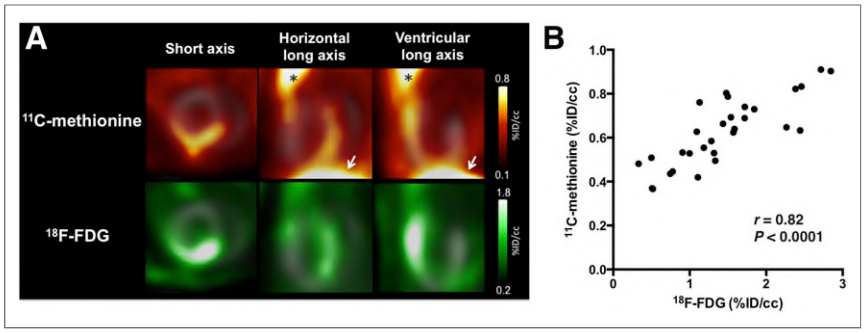

FIGURE 4. (A) Representative ^{11}C-methionine and ^{18}F-FDG PET images from EAM rat. Colocalization of focal myocardial uptake of both ^{11}C-methionine and ^{18}F-FDG is shown. Extracardiac ^{11}C-methionine uptake was noted in thymus (asterisk) and liver (arrowheads). Gray scale images serve as reference for location of heart. (B) In vivo, a strong correlation between cardiac tracer signals of ^{11}C-methionine and ^{18}F-FDG was found.

A rather strong focal cardiac uptake of ^{11}C-methionine could be observed in our PET imaging studies, indicating the feasibility of in vivo detection of myocardial inflammation. No conspicuous physiologic uptake of ^{11}C-methionine was observed in the hearts or lungs of our rats; however, the tracer was found to accumulate in the liver and the thymus. In our dynamic PET study, focal ^{11}C-methionine accumulation in the myocardium was readily visualized, remaining stable until the end of the scan together with a rapid clearance of the blood-pool activity, thus minimizing the signal-to-noise ratio for cardiac imaging.

^{18}F-FDG is the most commonly used PET tracer for assessing inflammation, including sarcoidosis (*36*), postmyocardial infarction (*37*), and other acute and chronic inflammatory conditions (*38,39*). Therefore, we performed a side-by-side comparison between ^{11}C/^{14}C-methionine and ^{18}F-FDG in ex vivo and in vivo experiments. Our ex vivo dual-tracer autoradiography analysis results indicated an excellent positive correlation between the accumulation of ^{14}C-methionine and uptake of ^{18}F-FDG in immunohistologically confirmed inflammatory myocardial lesions; moreover, these findings were consistent with the results from our in vivo PET experiments. Thus, both ^{18}F-FDG and ^{11}C-methionine PET appear suitable for use in diagnosing cardiac inflammatory processes. On the other hand, ^{18}F-FDG PET has the advantages of better contrast between inflamed and noninflamed myocardial areas and lower physiologic uptake in the liver and the thymus. However, physiologic myocardial background activity is sometimes difficult to suppress, especially in patients with heart failure, thereby special preparations such as fasting for prolonged periods, taking high-fat meals, and administering heparin would be necessary before performing ^{18}F-FDG PET (*40,41*). In our rat experiments, we minimized physiologic cardiac tracer uptake by implementing long fasting periods before the scans and by avoiding anesthesia during the distribution period of intraperitoneally injected ^{18}F-FDG. ^{11}C-methionine PET has an advantage over ^{18}F-FDG PET on this point because of the lack of ^{11}C-methionine uptake in the healthy myocardium, as shown in our analyses. Further evaluation is needed to assess which tracer is preferred in a variety of clinical practice settings.

CONCLUSION

Using a rat model of autoimmune myocarditis, here we demonstrate the feasibility of ^{11}C-methionine imaging for the detection of cardiac inflammation. ^{11}C/^{14}C-methionine accumulation colocalized with histologically confirmed cardiac inflammatory lesions and ^{18}F-FDG uptake, indicating that ^{11}C-methionine PET might represent a novel promising imaging modality for the noninvasive diagnosis of myocarditis also in human patients. However, further in-depth assessment of this tracer in large animal models or clinical trials is warranted.

DISCLOSURE

The costs of publication of this article were defrayed in part by the payment of page charges. Therefore, and solely to indicate this fact, this article is hereby marked "advertisement" in accordance with 18 USC section 1734. This work was supported by the Competence Network of Heart Failure funded by the Integrated Research and Treatment Center (IFB) of the Federal Ministry of Education and Research (BMBF) and German Research Council (DFG grant HI 1789/2-1). Yoshifumi Maya is an employee of Nihon Medi-Physics Co., Ltd. No other potential conflict of interest relevant to this article was reported.

ACKNOWLEDGMENTS

We thank Dr. Tomoyoshi Yanagisawa, Kitasato University School of Medicine, Sagamihara, Japan, for sharing his knowledge with respect to the here described EAM rat model.

REFERENCES

1. Doolan A, Langlois N, Semsarian C. Causes of sudden cardiac death in young Australians. *Med J Aust.* 2004;180:110–112.
2. Cooper LT Jr. Myocarditis. *N Engl J Med.* 2009;360:1526–1538.
3. Kindermann I, Barth C, Mahfoud F, et al. Update on myocarditis. *J Am Coll Cardiol.* 2012;59:779–792.
4. Kawai C. From myocarditis to cardiomyopathy: mechanisms of inflammation and cell death—learning from the past for the future. *Circulation.* 1999;99:1091–1100.
5. Caforio AL, Marcolongo R, Basso C, Iliceto S. Clinical presentation and diagnosis of myocarditis. *Heart.* 2015;101:1332–1344.
6. Cooper LT, Baughman KL, Feldman AM, et al. The role of endomyocardial biopsy in the management of cardiovascular disease: a scientific statement from the American Heart Association, the American College of Cardiology, and the European Society of Cardiology Endorsed by the Heart Failure Society of America and the Heart Failure Association of the European Society of Cardiology. *Eur Heart J.* 2007;28:3076–3093.
7. Friedrich MG, Sechtem U, Schulz-Menger J, et al. Cardiovascular magnetic resonance in myocarditis: a JACC white paper. *J Am Coll Cardiol.* 2009;53:1475–1487.
8. Abdel-Aty H, Boye P, Zagrosek A, et al. Diagnostic performance of cardiovascular magnetic resonance in patients with suspected acute myocarditis: comparison of different approaches. *J Am Coll Cardiol.* 2005;45:1815–1822.
9. Abdel-Aty H, Zagrosek A, Schulz-Menger J, et al. Delayed enhancement and T2-weighted cardiovascular magnetic resonance imaging differentiate acute from chronic myocardial infarction. *Circulation.* 2004;109:2411–2416.
10. Thavendiranathan P, Walls M, Giri S, et al. Improved detection of myocardial involvement in acute inflammatory cardiomyopathies using T2 mapping. *Circ Cardiovasc Imaging.* 2012;5:102–110.
11. Kim RJ, Wu E, Rafael A, et al. The use of contrast-enhanced magnetic resonance imaging to identify reversible myocardial dysfunction. *N Engl J Med.* 2000;343:1445–1453.
12. Grün S, Schumm J, Greulich S, et al. Long-term follow-up of biopsy-proven viral myocarditis: predictors of mortality and incomplete recovery. *J Am Coll Cardiol.* 2012;59:1604–1615.

13. Bengel FM, Higuchi T, Javadi MS, Lautamaki R. Cardiac positron emission tomography. *J Am Coll Cardiol.* 2009;54:1–15.
14. Glaudemans AW, Enting RH, Heesters MA, et al. Value of ^{11}C-methionine PET in imaging brain tumours and metastases. *Eur J Nucl Med Mol Imaging.* 2013;40:615–635.
15. Lückerath K, Lapa C, Albert C, et al. ^{11}C-methionine-PET: a novel and sensitive tool for monitoring of early response to treatment in multiple myeloma. *Oncotarget.* 2015;6:8418–8429.
16. Morooka M, Kubota K, Kadowaki H, et al. ^{11}C-methionine PET of acute myocardial infarction. *J Nucl Med.* 2009;50:1283–1287.
17. Taki J, Wakabayashi H, Inaki A, et al. ^{14}C-methionine uptake as a potential marker of inflammatory processes after myocardial ischemia and reperfusion. *J Nucl Med.* 2013;54:431–436.
18. Kubota R, Kubota K, Yamada S, et al. Methionine uptake by tumor tissue: a microautoradiographic comparison with FDG. *J Nucl Med.* 1995;36:484–492.
19. Oka S, Okudaira H, Ono M, et al. Differences in transport mechanisms of trans-1-amino-3-[^{18}F]fluorocyclobutanecarboxylic acid in inflammation, prostate cancer, and glioma cells: comparison with L-[methyl-^{11}C]methionine and 2-deoxy-2-[^{18}F]fluoro-D-glucose. *Mol Imaging Biol.* 2014;16:322–329.
20. *Guide for the Care and Use of Laboratory Animals.* Bethesda, MD: National Institutes of Health; 1985. NIH publication 85-23.
21. Lückerath K, Lapa C, Spahmann A, et al. Targeting paraprotein biosynthesis for non-invasive characterization of myeloma biology. *PLoS One.* 2013;8: e84840.
22. Madar I, Ravert HT, Du Y, et al. Characterization of uptake of the new PET imaging compound ^{18}F-fluorobenzyl triphenyl phosphonium in dog myocardium. *J Nucl Med.* 2006;47:1359–1366.
23. Higuchi T, Fukushima K, Rischpler C, et al. Stable delineation of the ischemic area by the PET perfusion tracer ^{18}F-fluorobenzyl triphenyl phosphonium after transient coronary occlusion. *J Nucl Med.* 2011;52:965–969.
24. Kodama M, Matsumoto Y, Fujiwara M, Masani F, Izumi T, Shibata A. A novel experimental model of giant cell myocarditis induced in rats by immunization with cardiac myosin fraction. *Clin Immunol Immunopathol.* 1990;57:250–262.
25. Schmerler P, Jeuthe S, O h-Ici D, et al. Mortality and morbidity in different immunization protocols for experimental autoimmune myocarditis in rats. *Acta Physiol (Oxf).* 2014;210:889–898.
26. Werner RA, Maya Y, Rischpler C, et al. Sympathetic nerve damage and restoration after ischemia-reperfusion injury as assessed by ^{11}C-hydroxyephedrine. *Eur J Nucl Med Mol Imaging.* 2016;43:312–318.
27. Loening AM, Gambhir SS. AMIDE: a free software tool for multimodality medical image analysis. *Mol Imaging.* 2003;2:131–137.
28. Suzuki J, Ogawa M, Watanabe R, et al. Autoimmune giant cell myocarditis: clinical characteristics, experimental models and future treatments. *Expert Opin Ther Targets.* 2011;15:1163–1172.
29. Myers JM, Fairweather D, Huber SA, Cunningham MW. Autoimmune myocarditis, valvulitis, and cardiomyopathy. *Curr Protoc Immunol.* 2013;101:15.14.1–15.14.51.
30. Kodama M, Zhang S, Hanawa H, Shibata A. Immunohistochemical characterization of infiltrating mononuclear cells in the rat heart with experimental autoimmune giant cell myocarditis. *Clin Exp Immunol.* 1992;90:330–335.
31. Hanawa H, Tsuchida M, Matsumoto Y, et al. Characterization of T cells infiltrating the heart in rats with experimental autoimmune myocarditis: their similarity to extrathymic T cells in mice and the site of proliferation. *J Immunol.* 1993;150:5682–5695.
32. Moon H, Park HE, Kang J, et al. Noninvasive assessment of myocardial inflammation by cardiovascular magnetic resonance in a rat model of experimental autoimmune myocarditis. *Circulation.* 2012;125:2603–2612.
33. Fairweather D, Frisancho-Kiss S, Rose NR. Viruses as adjuvants for autoimmunity: evidence from Coxsackievirus-induced myocarditis. *Rev Med Virol.* 2005;15:17–27.
34. Fairweather D, Rose NR. Coxsackievirus-induced myocarditis in mice: a model of autoimmune disease for studying immunotoxicity. *Methods.* 2007;41:118–122.
35. Stumpf WE. Drug localization and targeting with receptor microscopic autoradiography. *J Pharmacol Toxicol Methods.* 2005;51:25–40.
36. Blankstein R, Osborne M, Naya M, et al. Cardiac positron emission tomography enhances prognostic assessments of patients with suspected cardiac sarcoidosis. *J Am Coll Cardiol.* 2014;63:329–336.
37. Lee WW, Marinelli B, van der Laan AM, et al. PET/MRI of inflammation in myocardial infarction. *J Am Coll Cardiol.* 2012;59:153–163.
38. Vaidyanathan S, Patel CN, Scarsbrook AF, Chowdhury FU. FDG PET/CT in infection and inflammation: current and emerging clinical applications. *Clin Radiol.* 2015;70:787–800.
39. Ozawa K, Funabashi N, Daimon M, et al. Determination of optimum periods between onset of suspected acute myocarditis and ^{18}F-fluorodeoxyglucose positron emission tomography in the diagnosis of inflammatory left ventricular myocardium. *Int J Cardiol.* 2013;169:196–200.
40. Cheng VY, Slomka PJ, Ahlen M, Thomson LE, Waxman AD, Berman DS. Impact of carbohydrate restriction with and without fatty acid loading on myocardial ^{18}F-FDG uptake during PET: a randomized controlled trial. *J Nucl Cardiol.* 2010;17:286–291.
41. Wykrzykowska J, Lehman S, Williams G, et al. Imaging of inflamed and vulnerable plaque in coronary arteries with ^{18}F-FDG PET/CT in patients with suppression of myocardial uptake using a low-carbohydrate, high-fat preparation. *J Nucl Med.* 2009;50:563–568.